A novel sensing layer based on metal–organic framework UiO-66 modified with TiO$_2$–graphene oxide: application to rapid, sensitive and simultaneous determination of paraoxon and chlorpyrifos

Nashmil Karimian,[a] Hanieh Fakhri,[b] Salimeh Amidi,[c] Ali Hajian,[d] Fabiana Arduini[e] and Hasan Bagheri [ID] *[b]

In this paper, a novel enzymeless electrochemical sensor with high sensitivity was constructed based on TiO$_2$ functionalized graphene oxide@UiO-66 (TGO@UiO-66) for simultaneous detection of paraoxon and chlorpyrifos. TGO@UiO-66 for electrode modification possesses good conductivity and a distinctive structure, which promotes the electron transfer rate and improves the efficiency of electrochemical sensors. In this work, a TGO@UiO-66 modified glassy carbon electrode (TGO@UiO-66/GCE) was used for simultaneous determination of paraoxon and chlorpyrifos. The square wave voltammogram of TGO@UiO-66/GCE in the presence of paraoxon and chlorpyrifos showed two characteristic cathodic peaks at −0.45 and −1.3 V (*vs.* Ag/AgCl). Also, excellent electrochemical characteristics of the proposed sensor were evidenced by impedance and cyclic voltammetry studies in a Fe(CN)$_6^{4-/3-}$ solution. Different experimental parameters such as the type of electrolyte, pH of the electrolyte, and scan rate were optimized, and calibration curves were plotted under the optimal conditions. The designed sensor exhibited low detection limits of 0.2 and 1.0 nM within the linear ranges of 1.0–100.0 nM and 5.0–300.0 nM for paraoxon and chlorpyrifos, respectively. The developed sensor was successfully applied to pesticide residue monitoring in vegetable and water samples.

Introduction

Organophosphorus compounds (OPs) are a diverse group of pesticides that are widely used in modern agriculture for controlling pests in agricultural food commodities and ornamental plants.[1–4] OPs have been considered toxic to humans and even a low dermal, respiratory, or oral exposure to an OP pesticide or nerve agent causes inhibition of acetylcholinesterase at nerve synapses and therefore, can result in respiratory lesions, paralysis, or even death.[5,6] For environmental protection and security of public health, accurate assessment of pesticides in water, plants, soils, and nutrition is a formidable challenge.

Paraoxon (POX) and chlorpyrifos (CPF) are two important OPs which are mainly used as insecticide products in crop protection and households.[7,8] POX is one the most toxic pesticides that can be absorbed through the skin. Also, it has been used as an ophthalmological drug against glaucoma and an assassination weapon. CPF is moderately toxic to humans as a neurotoxin and endocrine disruptor and is especially harmful to pregnant women and infants.[9] Therefore, over recent years significant effort has gone into the development of efficient and sensitive methods such as liquid or gas chromatography (HPLC or GC) for detection of these pesticides. However, these techniques are not appropriate for *in situ* and real-time detection and require expensive equipment and highly trained personnel for their operation as well as time-consuming extraction and cleanup steps.

Electrochemical techniques with high sensitivity, low-cost, rapid response, and simplicity have arisen as a promising analytical tool for the detection of OPs. Of this subject, enzymatic biosensors and immunosensors are commonly employed for the determination of POX and CPF.[10–16] Although enzyme-based sensors in most cases exhibit excellent performance for detection of organophosphorus insecticides, there are still serious problems and limitations

[a] Research and Development Department, Farin Behbood Tashkhis LTD, Tehran, Iran
[b] Chemical Injuries Research Center, Systems Biology and Poisonings Institute, Baqiyatallah University of Medical Sciences, Tehran, Iran. E-mail: h.bagheri@bmsu.ac.ir
[c] Department of Medicinal Chemistry, School of Pharmacy, Shahid Beheshti University of Medical Sciences, Tehran, Iran
[d] Institute of Sensor and Actuator Systems, TU Wien, 1040 Vienna, Austria
[e] Department of Chemical Science and Technologies, University of Rome Tor Vergata, Via della Ricerca Scientifica, 00133 Rome, Italy

regarding their fabrication, storage, and stability while non-enzyme sensors are not associated with these limitations.

To date, a wide range of electrode modifiers such as metal nanoparticles,[17] conducting polymers,[18] carbon nanotubes,[19] graphene[20] and ordered mesoporous carbon[21] have received increasing attention in electrochemical sensors. Recently, metal–organic frameworks (MOFs), an emerging class of advanced porous materials which consist of metal ions/clusters connected by organic linker groups, have attracted significant attention in applied sciences. Unique properties of MOFs, such as their high specific surface area, ordered crystalline structure, permanent porosity, excellent thermal stability, and tailorability have made them a major topic in various applications. In particular, a zirconium-based MOF, UiO-66, due to its excellent thermal, aqueous and acid stability, versatile syntheses, and ease of modification, is known as an exceptional candidate in various fields such as catalysis, separation, and gas storage.[22,23]

However, the poor electronic conductivity of MOFs has limited their electrochemical applications. To address this issue and in order to improve their electrochemical properties, MOF-based composites containing conducting substrates such as metal oxide, graphene oxide (GO), and carbon nanotubes have been proposed. The reported studies confirm the excellent improvement of electrochemical properties while using metal oxide/graphene (oxide) composites. For example, an improvement in electrochemical behavior using graphene and mesoporous TiO_2 for simultaneous sensing of sunset yellow and tartrazine has been reported.[24] Moreover, sensitive and selective sensing of 8-hydroxy-2′-deoxyguanosine by a ZnO/GO-based electrode has been reported.[25] In another study, significant electrocatalytic activity was obtained by TiO_2/graphene for simultaneous detection of adenine and guanine.[26]

By considering the high performance of each individual component, and taking the high affinity of nano TiO_2 for phosphate groups (such as in POX and CPF) into account,[27] the main aim of the present work is modification of a glassy carbon electrode with the TiO_2@GO/UiO-66 nanocomposite which is prepared through a straightforward sonication method and this novel sensing platform has been employed for the simultaneous determination of POX and CPF in real samples.

Experimental

Reagents and apparatus

POX and CPF were provided by Sigma-Aldrich. Zirconium(IV) chloride ($ZrCl_4$), 2-aminoterephthalic acid, 2-propanol, titanium isopropoxide, and graphite were provided by Sigma-Aldrich. All other chemicals and reagents used in this work were of analytical grade and used as received without further purification. The stock solutions of pesticides (1.0×10^{-3} M) were prepared in acetonitrile. The supporting electrolyte was a solution of 0.1 M Britton–Robinson (B–R) buffer/acetonitrile (9/1) that changed from a pH of 1.0 to 10.0.

All electrochemical experiments were carried out using an Ivium potentiostat/galvanostat (Vertex, Ivium Technologies, The Netherlands). The electrochemical cell consisted of the different modified electrodes as the working electrode, and Ag/AgCl and platinum wire were applied as the reference and counter electrodes, respectively. All voltammetric measurements were performed at room temperature. The X-ray diffraction (XRD) spectra of the prepared samples were obtained using an X-ray powder diffractometer (38066 Riva, d/G. *via* M. Misone, 11/D (TN) Italy), using Kα radiation (λ = 1.5418 Å). FT-IR spectra were recorded in the range of 4000–500 cm^{-1} on a PerkinElmer Spectrum 100 FT-IR spectrometer and KBr pellets were used to prepare the samples for FT-IR measurements. The morphology and size of the nanoparticles were characterized by scanning electron microscopy (SEM) and transmission electron microscopy (TEM, Philips CM10, operating at 100 kV), respectively.

Synthesis of TGO@UiO-66

Synthesis of UiO-66. UiO-66 was prepared according to a previously reported method.[28] In brief, 38.0 mg of $ZrCl_4$ was dissolved in 36.0 mL of dimethylformamide (DMF). Then, 27.0 mg of terephthalic acid was added to the mixture and sonicated for 10 min. In the next step, the mixture was placed in an autoclave and heated at 120 °C for 24 h. The precipitate was collected by centrifugation and washed several times with DMF and methanol. The final precipitate was dried at 100 °C for 24 h.

Synthesis of TiO_2/GO. A mixture of 2-propanol (10.0 mL) and titanium isopropoxide (3.0 mL) was stirred for 5 min. Then, 5.0 mL H_2O was added to the mixture and stirred for 1 h. This resulting suspension was placed in an oven at 100 °C for 12 h. The separated powder was calcined at 500 °C for 4 h.

The modified Hummers method was employed for synthesis of GO as reported in ref. 29. 100.0 mg of GO was dispersed in a solution comprising 40.0 mL ethanol and 20.0 mL water.

Then, 50.0 mg of TiO_2 was added to the mixture and stirred for 30 min. Finally, the mixture was transferred to an autoclave and heated at 120 °C for 12 h. The final product was washed with ethanol and water three times. The obtained powder was dried at 70 °C for 6 h. This product which was composed of TiO_2 and GO was designated as TGO.

Synthesis of TGO@UiO-66. The composite material TGO@UiO-66 was synthesized by a facile method similar to the method employed in the preparation of UiO-66. Firstly, a solution of TGO (10.0 mg in 30.0 mL DMF) was sonicated for 60 min. Then, 38.0 mg $Zr(NO_3)$ was added to it and sonicated for 5 min. After that, 27.0 mg 2-bromoterephthalic acid (H_2BDC) was added into the mixture.

The resulting suspension was sonicated for 50 min, and the final mixture was transferred into an autoclave and maintained at 120 °C for 12 h. Then, the obtained sample was washed with methanol and DMF and dried at 70 °C for 8 h.

Preparation of the modified electrode

The bare glassy carbon electrode (GCE) was hand polished with 3.0 and 0.05 μm alumina powders on the mirror-like surface, then sonicated in ethanol and rinsed thoroughly with double distilled water. The TGO@UiO-66/GCE was prepared by dropping 6.0 μL of TGO@UiO-66/ethanol suspension onto the bare GCE surface. Then the modified electrode was dried in the air and finally was used as the working electrode.

Electrochemical measurements

Square wave voltammetry (SWV) was recorded to determine OP pesticides in 0.1 M BR (pH = 5) from −0.1 to −2.0 V with a step potential of 10 mV, an amplitude of 10 mV, and a frequency of 80 Hz. Before the experiment was carried out, the electrolyte solution was purged with nitrogen for 10 min. All measurements were performed at room temperature.

Sample preparation

To evaluate the performance of the designed sensor in the determination of POX and CPF in real samples, tap water, and vegetable samples were investigated. Vegetable samples (celery, lettuce, and cabbage) were obtained from local markets in Tehran. The samples were precisely weighed and were cut into small pieces in a flask containing 30.0 mL ethanol. The mixture was sonicated for 50 min and then was centrifuged, and the supernatant was collected for analysis. Through the standard addition method, different amounts of POX and CPF were spiked to obtain concentrations in the linear range of the calibration curve.

Results and discussion

Characterization of TGO@UiO-66

The SEM micrograph in Fig. 1a shows the smooth and sheet-like morphology of GO. Fig. 1b and c confirm the formation of UiO-66 with a uniform size between 200 and 250 nm which is in agreement with the previously reported work.[30] As seen in Fig. 1d, the surface of GO is covered by TiO_2 nanoparticles and UiO-66 as an octahedral structure inserted between agglomerated layers of TGO (TiO_2 functionalized GO). The agglomeration of TGO can be explained by the strong interaction and dispersive power of GO layers.[31,32]

FT-IR spectra of the synthesized samples are shown in Fig. 2A. In Fig. 2A(a), the characteristic peaks at 3965, 1739, 1615, and 1229 cm^{-1} are attributed to the O–H stretching, C=O stretching, C=C stretching and C–O stretching vibrations, respectively. The peak located at 510 cm^{-1} was assigned to the Ti–O stretching vibration that confirmed immobilization of TiO_2 on GO (Fig. 2A(b)). The main characteristic peaks belonging to UiO-66 are observed at 1370 cm^{-1} and 1568 cm^{-1} which
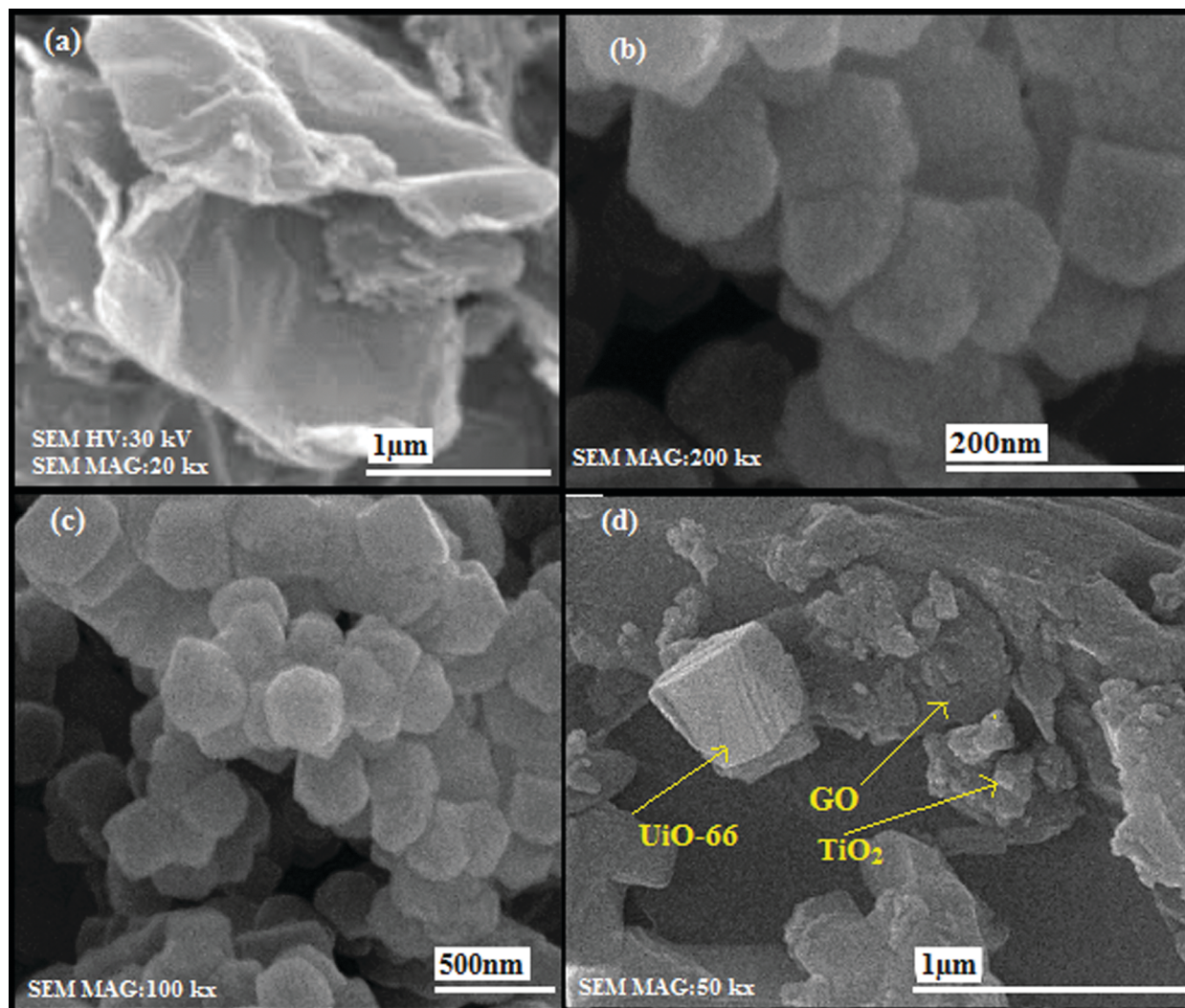

Fig. 1 SEM images of (a) GO, (b and c) UiO-66, and (d) TGO@UiO-66.

corresponded to the C=C stretching vibration of the benzene ring and OCO respectively. Moreover, characteristic bands with low intensity are located at 486–736 cm^{-1} which can be assigned to the combination of Zr–O modes with OH and CH bending.[33]

As can be seen, the structural features of UiO-66 are preserved in the presence of TG (Fig. 2A(c)). In Fig. 2A(d) the presence of GO in the nanocomposite spectra is not visible easily due to the overlap with other peaks. The change and shift of peaks belong to pure UiO-66 compared to the nanocomposite can be assigned to interactions between components of the composite.

The phase purity of prepared materials is investigated by XRD analysis. Fig. 2B shows XRD patterns of UiO-66, T, GO and TG@UiO-66. As shown in Fig. 2B, the main peak at 11.9 A is assigned to the (001) reflection of GO.[34] In the XRD pattern of bare T, only the anataze phase is detected without any impurities. In the case of UiO-66, the observed diffraction peaks are in

agreement with reported work.[30] After UiO-66 modification by TG, all diffractions belong to UiO-66 were well preserved, indicating that the presence of TG did not disturb the formation of crystals of UiO-66.[35–37] Notably, the broadened diffraction peaks indicated that T on the surface of GO (in the TG@UiO-66 matrix) has a low degree of crystallinity.[38] Furthermore, the absence of GO diffraction is due to the insertion of UiO-66 between TG layers that effectively reduces the van der Waals binding energy between the GO sheets and improves the layer exfoliation and also high dispersion of TG layers during the nanocomposite preparation can be another reason for this observation.[39–41] These concepts can be verified by FT-IR and SEM analyses.

In order to investigate the samples' porosity, N$_2$ adsorption–desorption analysis of UiO-66 (Fig. 2C(a)) and TG@UiO-66 (Fig. 2C(b)) was performed at 77 K and 1 bar. Both samples show type IV isotherms and a narrow pore size distribution.
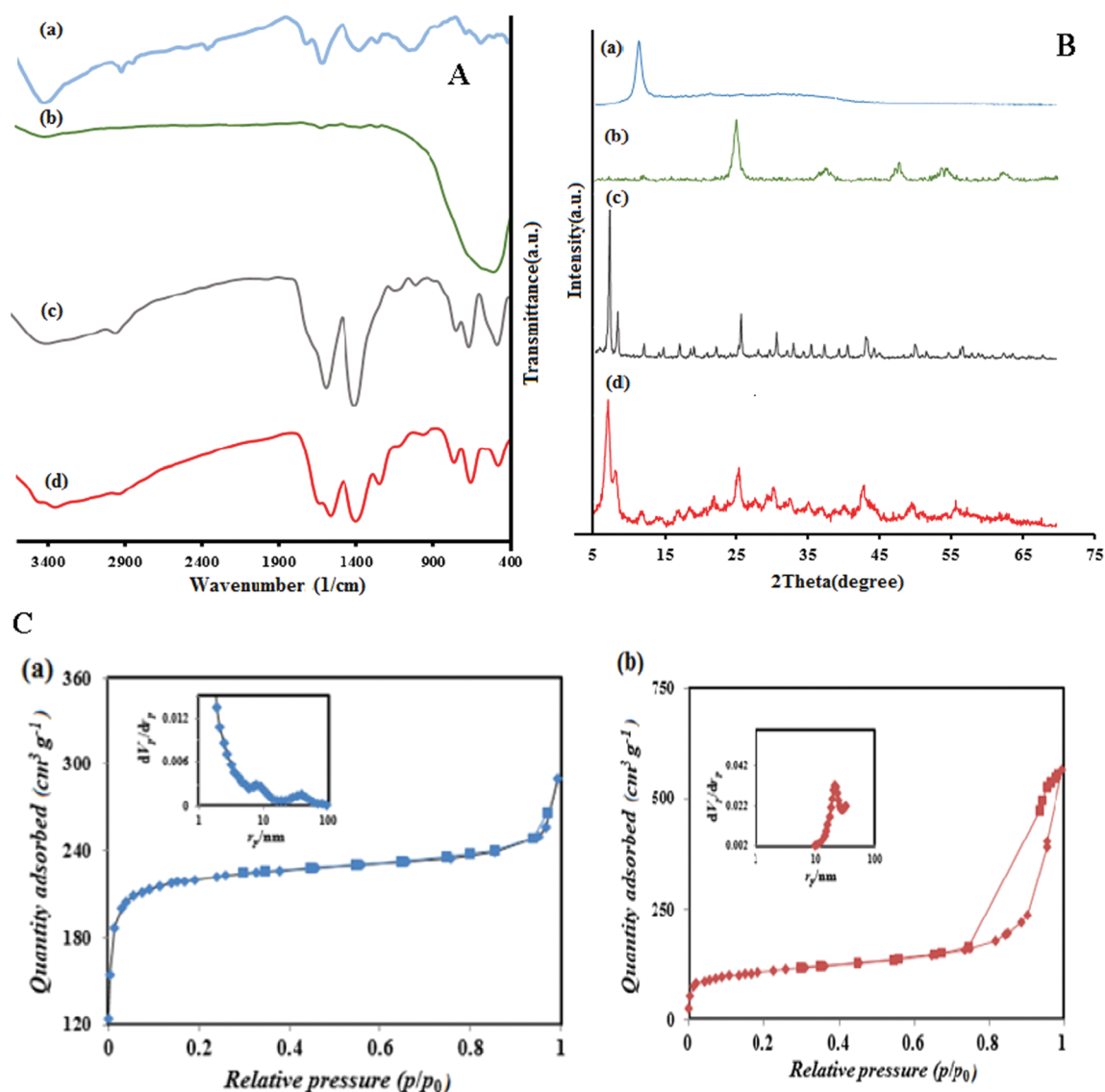

Fig. 2 (A) FT-IR spectra of (a) GO, (b) TiO$_2$, (c) UiO-66, and (d) TGO@UiO-66, (B) XRD of (a) GO, (b) TiO$_2$, (c) UiO-66, and (d) TGO@UiO-66, and (C) N$_2$ adsorption–desorption of (a) UiO-66 and (b) TGO@UiO-66.

Type IV isotherms are classified as mesoporous solids. Inflections of the isotherms, attributed to the capillary condensation of nitrogen in mesopores, are observed in the P/P_0 region of 0.75–0.85, with H_4 and H_2 type hysteresis loops for UiO-66 and TG@UiO-66, respectively. By modification of UiO-66 by TGO, the pore volume and surface area are altered from 0.44 cm^3 g^{-1} and 856 m^2 g^{-1} to 0.84 cm^3 g^{-1} and 379 m^2 g^{-1}. The reduction of the specific surface area is associated with the distribution of TGO in the internal surfaces of UiO-66 which was confirmed by the XRD and FT-IR analyses. Furthermore, it can be suggested that TGO supplies new crystallization sites for UiO-66 which lead to the improved porosity.[42]

Electrochemical impedance spectroscopy

Electrochemical impedance spectroscopy (EIS) was used as an efficient technique to monitor the change in the electrical properties of the electrode surface during the sensor fabrication process. The equivalent circuit model fitted to the impedance data has components R_{et}, the resistance of the electron transfer between the solution and the electrode surface; ZW, the Warburg element; CPE, the constant phase element, and R_s, the solution resistance. EIS was performed using TGO@UiO-66/GCE in a 0.1 M KCl solution containing 1×10^{-5} M $[Fe(CN)_6]^{3-/4-}$ and then fitting of spectra was done in Fig. 3A. As shown in Nyquist impedance circular fitting plots, the coating of TG@UiO-66 on GCE decreases R_{et} compared with the bare GCE (1.43 kΩ), confirming that the large effective surface area has enhanced the electron transfer on the electrode surface.

In order to acquire the electrochemical active surface areas of both GCE and TGO@UiO-66/GCE using the Randles–Sevcik equation (eqn (1)) and to confirm the result of EIS, cyclic voltammetry was conducted in $K_4[Fe(CN)_6]$ as a redox probe at different scan rates (Fig. 3B and C):

$$I_p = (2.69 \times 105)n^{3/2}AC^{\star}D^{1/2}\nu^{1/2} \qquad (1)$$

where n, A, $C^{\star}$, D, and ν are the number of electrons, electrode area, concentration, diffusion coefficient, and scan rate, respectively.

Accordingly, a linear correlation was observed between the peak current and the square root of the scan rate, and the surface electrode area for TGO@UiO-66/GCE (0.13 cm^2) and bare GCE (0.04 cm^2) can be calculated from the slope of eqn (1). The large active surface area of TGO@UiO-66/GCE was attributed to the highly porous structure of UiO-66 and unique properties of GO and TiO$_2$ nanoparticles.

Electrochemical determination of POX and CPF at TGO@UiO-66/GCE and the effect of pH

SWVs of the bare GCE and TG@UiO-66/GCE were recorded in the electrochemical cell containing 0.1 M BR buffer (pH = 5) with 50.0 nM POX and 50.0 nM CPF. As shown in Fig. 4, the SWV exhibited two reduction peaks of POX and CPF at −0.45 and −1.35 V vs. Ag/AgCl which can be attributed to the electrochemical reduction of POX and CPF.[16,43] The GCEs modified using TiO$_2$ (T), graphene oxide (GO), UiO-66 and combinations of TiO$_2$–graphene oxide (TGO), UiO-66–graphene oxide (GO@UiO-66) and UiO-66–graphene oxide–TiO$_2$ (TGO@UiO-66) were examined for detection of the prepared samples and their results are shown in Fig. 4. As can been seen, the peak currents were increased when TiO$_2$ and GO were used as a modifier in comparison to bare GCE and UiO-66/GCE. The enhancement
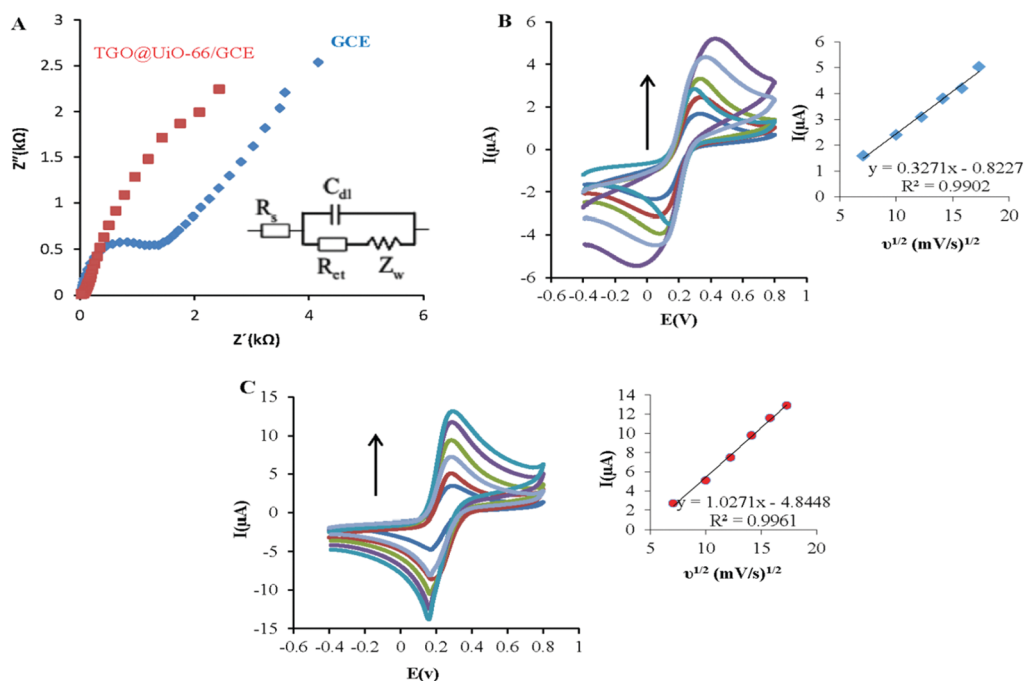

Fig. 3 (A) Electrochemical impedance spectroscopy of 0.1 M KCl containing 1×10^{-5} M Fe(CN)$_6^{3-/4-}$ for bare GCE and TGO@UiO-66/GCE, and cyclic voltammograms of 0.1 M KCl containing 1×10^{-5} M Fe(CN)$_6^{3-/4-}$ at different scan rates (50–350 mV s^{-1} from bottom to top) for (B) bare GCE and (C) TGO@UiO-66/GCE, inset: plots of peak current vs. $\nu^{1/2}$.
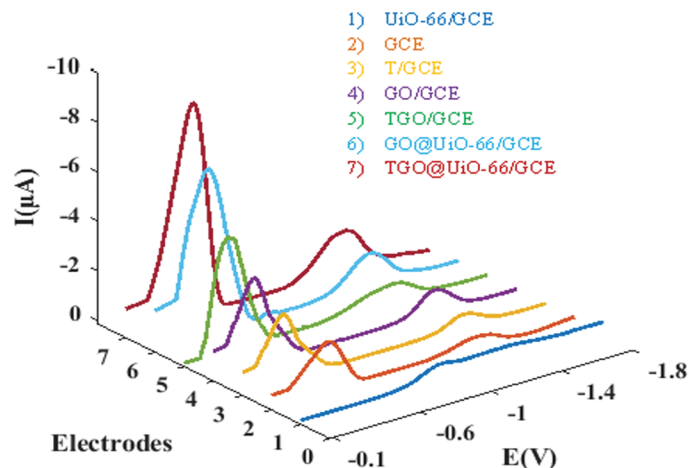
Fig. 4 SW voltammograms in the presence of 50 nM POX and 50 nM CPF in B−R buffer solution/acetonitrile (9/1) at pH = 5.0 on the surface of bare GCE and different modified electrodes.

in peak currents may be attributed to their high surface area and good electrical conductivity. Finally, the maximum response was achieved by TGO@UiO-66/GCE which indicated that TGO@UiO-66/GCE as a modifier not only facilitates the electron transfer kinetics but also increases the sensitivity of the electrode for pesticide monitoring which is due to the presence of all three species in the composite modifier. The high porosity and surface areas of MOFs are important elements to consider in optimizing the performance of the electrochemical assay. Although the attractive properties of MOFs suggest them as ideal materials for the surface modification of electrodes, the low conductivity is a major challenge for MOF-based electrochemical sensors. For improvement in the conductivity of MOF-electrochemical sensors, MOFs are usually combined with functional materials such as metal nanoparticles and carbon nanostructures. Consequently, MOF composites/hybrids have the advantages of both MOFs (high porosity with ordered crystalline pores and high stability) and other active materials (electrical and catalytic properties), and the electrochemical performances are enhanced. Also, TiO_2 inserted on GO (TGO/GCE) could increase the response of the designed sensor towards the targets compared to GO/GCE and GO@UiO-66/GCE due to the high affinity of nano-TiO_2 for phosphate groups and carboxylic groups can bind on the TiO_2 nanoparticles and enhance the electron transfer processes in the electrochemical sensing for detection of organophosphate pesticides.[27]

The effects of supporting electrolytes and pH were investigated using SWV of the peak potentials and peak currents of POX and CPF. TGO@UiO-66/GCE was used for POX (50.0 nM), and CPF (50.0 nM) reduction with different supporting electrolytes and the maximum response was obtained in 0.1 M BR buffer/acetonitrile (9/1). Then the response of TGO@UiO-66/GCE was investigated in 0.1 M BR buffer/acetonitrile (9/1) solutions containing 50.0 nM POX and 50.0 nM CPF at different pH values between 2.0 and 8.0 (Fig. 5A). The obtained results confirm the significant role of pH in the electrochemical reduction of POX and CPF. For both compounds, the highest

peak currents were obtained at pH = 5 and then decrease gradually. Thus, pH = 5.0 was considered as the optimum. Moreover, as can be observed in Fig. 5B, the peak potentials have shifted towards less negative values with decreasing pH value, and the following linear ranges were obtained for each compound:

$$E_{pa}(POX) = -0.0632pH - 1.2125 \ (R^2 = 0.9894)$$

$$E_{pa}(CPF) = -0.0557pH - 0.3871 \ (R^2 = 0.9902)$$

The slope values for the plots of E_{pa} vs. pH are close to the theoretical value of -0.059 V pH^{-1} for both POX and CPF which indicates the presence of an equal number of protons and electrons in their reduction processes, which is in agreement with the literature.[43,44]

The effect of the scan rate on the reduction peak currents of POX and CPF at TG@UiO-66/GCE were investigated by the CV technique, varying the scan rate from 10 to 400 mV s^{-1}. The linear dependence between the peak currents and the square root of scan rates ($\nu^{1/2}$) indicating the reductions kinetics of both pesticides was a diffusion-controlled process (Fig. 6). Also, good linearity was obtained between the logarithm of peak current (log I_{pc}) and logarithm of the scan rates (log ν) that the slope values are near to theoretical value of 0.5. The results confirmed reductions of these pesticides on designed sensor are diffusion-controlled processes.

Analytical performance of TGO@UiO-66/GCE for the detection of POX and CPF

Under the optimal conditions, different concentrations of POX and CPF were separately and simultaneously determined using TGO@UiO-66/GCE by the SWV technique. Fig. 7A shows the SWV recordings at various POX concentrations with a constant CPF concentration of 50.0 nM at TGO@UiO-66/GCE. The peak currents of POX increased with increasing concentration of POX in the range of 1.0 to 100.0 nM in the presence of CPF. The SWV
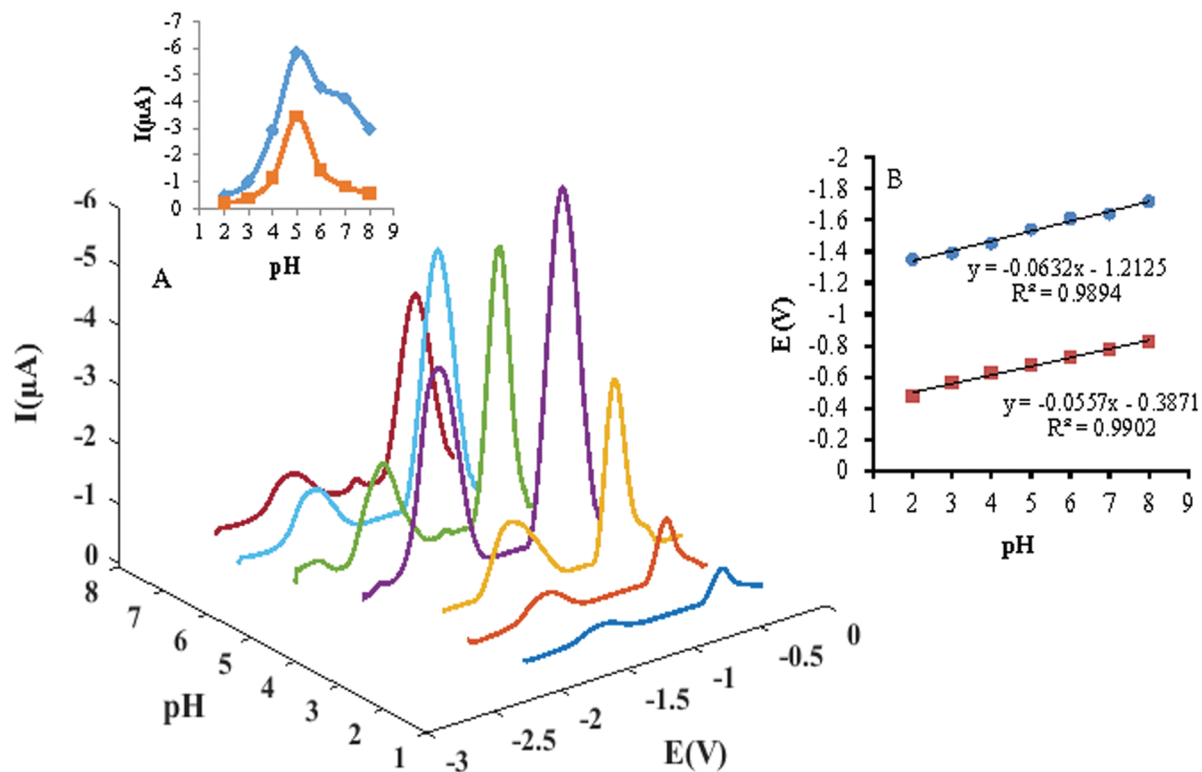
Fig. 5 (A) Cyclic voltammograms of B−R buffer solution containing 50 nM POX and 50 nM CPF in different pH (1−9), (B) plot of the anodic peak potential *vs.* pH of the solution.
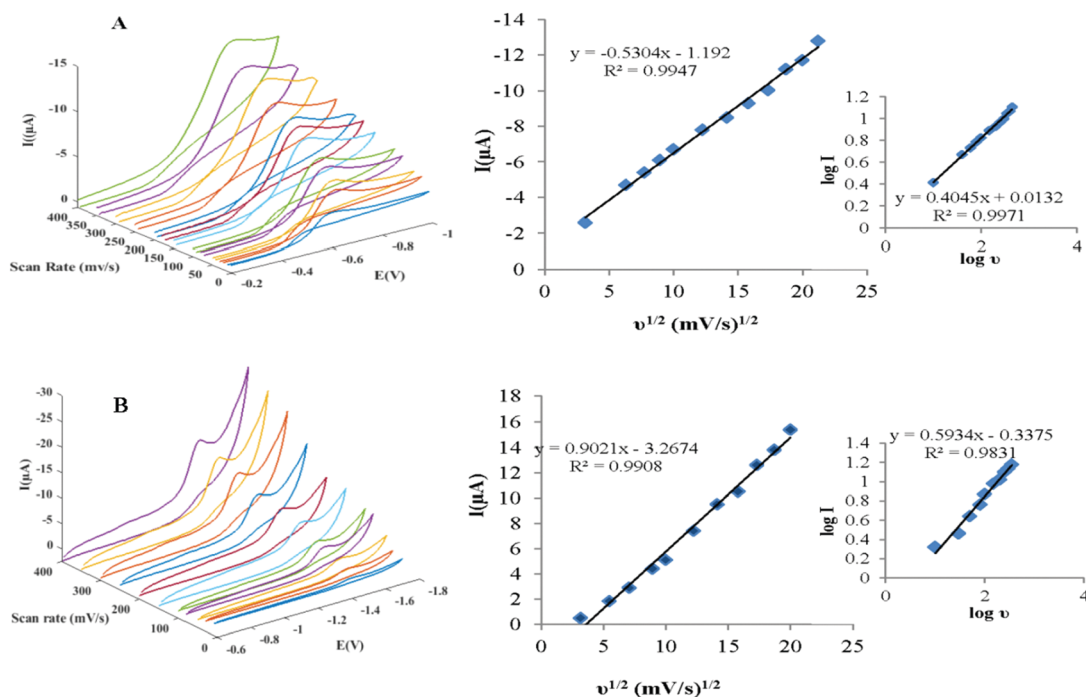

Fig. 6 Cyclic voltammograms of (A) 50 nM POX and (B) 50 nM CPF in B−R buffer solution (pH = 5.0) at different scan rates using TGO@UiO-66/GCE, plots of peak current *vs.* $\nu^{1/2}$ and log *I vs.* log *ν* (inset).

curves indicate that 50 nM CPF has no interference for the determination of POX.

In a similar way, the peak currents for CPF were increased by raising its concentration from 5.0 to 300.0 nM in the presence

of a constant POX concentration of 50.0 nM (Fig. 7B). Also, limits of detection (LOD) of 0.2 nM and 1.0 nM for POX and CPF were obtained, respectively. Fig. 7C shows the SWV responses of TGO@UiO-66/GCE in the 0.1 M BR solutions (pH = 5.0) containing various concentrations of POX (1.0 to 100.0 nM) and CPF (5.0 to 300.0). The linear equations were:

$$I_{pc}(POX) = 0.1277 - 0.3393(C_{pox}) \ (R^2 = 0.9966)$$

$$I_{pc}(CPF) = 0.1409 - 0.091(C_{CPF}) \ (R^2 = 0.9963)$$

The calculated LOD values were 0.22 nM and 1.2 nM for POX and CPF, respectively. These results are close to LOD values for individual compounds and indicate that the species do not interfere with each other during determination with a low LOD and in a broad linear range.

Furthermore, repeatability studies were performed for the simultaneous determination of POX and CPF in a BR solution containing 50.0 nM of each analyte. RSD values of 2.6% and 2.2% were obtained for POX and CPF, respectively, from 6 consecutive measurements on the same day.
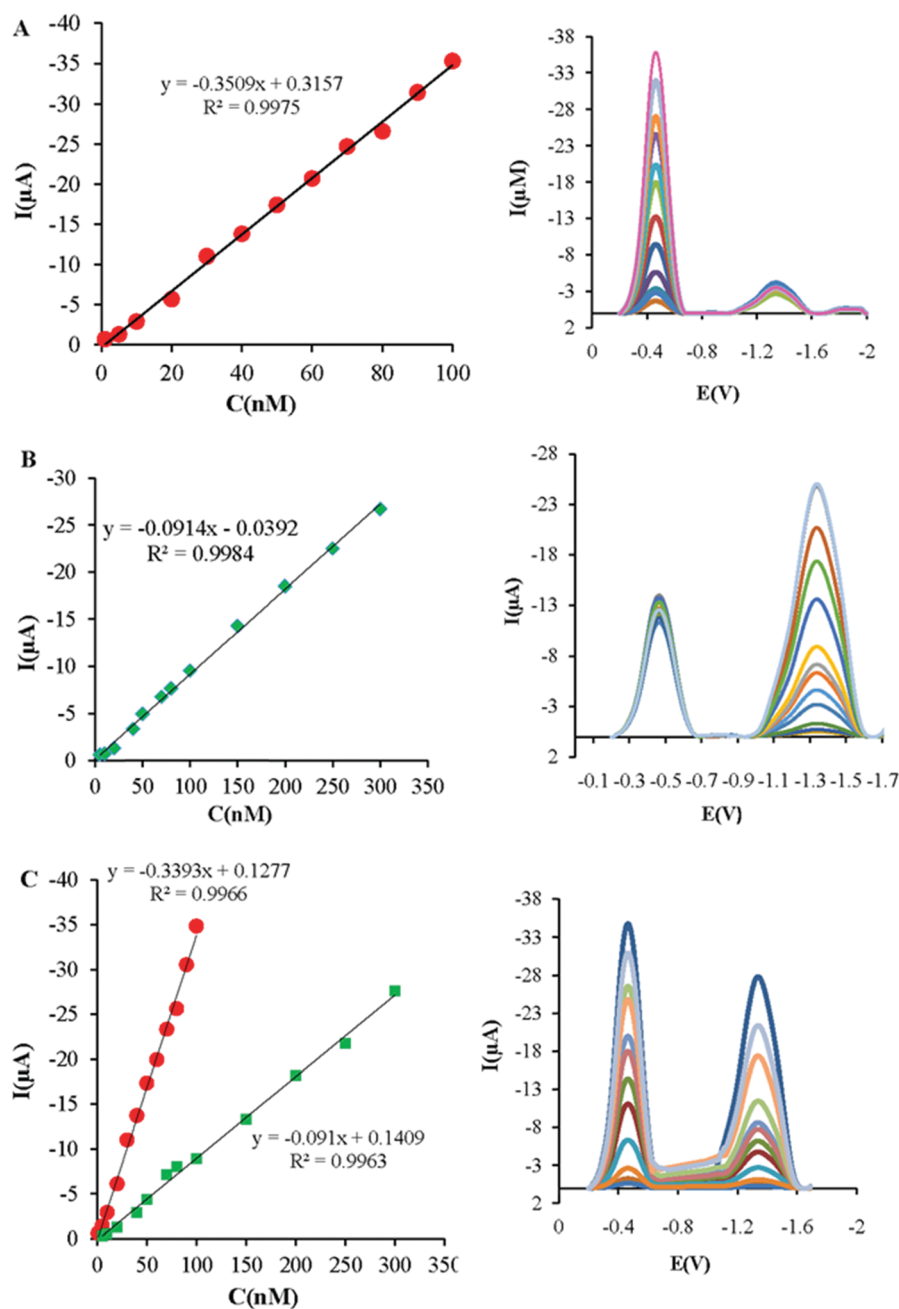

Fig. 7 SW voltammograms of (A) different concentrations of POX (1.0–100.0 nM) in the presence of 50.0 nM CPF, (B) different concentrations of CPF (5.0–300.0 nM) in the presence of 50.0 nM POX at TGO@UiO-66/GCE, and (C) different concentrations of 1.0–100.0 and 5.0–300.0 nM for POX and CPF in the B–R buffer solution (pH = 5.0).

The reproducibility of the proposed sensor was also investigated for five similarly fabricated individual electrodes. Relative standard deviations (RSDs) of less than 2.9% and 3.4% were obtained for POX and CPF, respectively, for the electrodes used in a BR solution containing 50.0 nM of POX and CPF.

The stability of TGO@UiO-66/GCE was also examined when electrodes were stored at room temperature for two weeks.

The peak current response to 50.0 nM of POX and CPF showed a 4.2% for POX and 4.6% for CPF decrease of the original response indicating the good stability of the proposed electrode.

Selectivity and interference study

The influences of common interfering substances and other pesticides in the presence of 50.0 nM of POX and CPF at TGO@UiO-66/GCE were evaluated. The tolerance limit was defined as the concentration of the interfering component that caused an error of less than $\pm5\%$ in the determination of the target analyte. The results showed that a 100-fold excess of inorganic ions such as Cl^-, SO_4^{2-}, CO_3^{2-}, NO_3^-, PO_4^{3-}, Cu^{2+}, Zn^{2+}, Pb^{2+}, Fe^{2+}, and Cd^{2+} caused an error of less than $\pm4\%$. Also, a 10 fold excess of diazinon, carbaryl, carbofuran, nitrite, parathion, nitrobenzene, sulfide, and fenamiphos, which have approximately similar structures to the target analytes, caused an error of less than $\pm5\%$ in the presence of 50.0 nM of POX and CPF. For parathion, two cathodic and anodic peaks were observed at -1.0 V and -0.06 V (vs. Ag/AgCl), respectively. Also, for nitrobenzene a reduction peak at -1.5 V as well as peaks at -0.45 and -1.3 V for POX and CPF were seen.

Therefore, these compounds do not interfere with the detection of POX and CPF, since the separation of reduction peak potentials was enough and TGO@UiO-66/GCE showed more selectivity toward POX and CPF than the other compounds. The oxidation of nitrite and sulfide occurred in the potential range of 0–1.4 V and did not influence the reduction signals of POX and CPF. Therefore, the fabricated sensor is free from interfering agents and is suitable for the simultaneous determination of POX and CPF in complex samples.

Real samples

To assess the practical applications, concentrations of POX and CPF using TGO@UiO-66/GCE with the standard addition method were determined in celery, lettuce and cabbage, and tap water samples. Table 1 shows the data gained by the proposed sensor which are highly satisfactory, indicating the reliability of TGO@UiO-66/GCE for the determination of POX and CPF in the different matrixes.

Conclusions

In brief, a novel enzymeless electrochemical sensor based on TiO_2 functionalized graphene oxide supported on UiO-66 was fabricated and used for individual and simultaneous determination of two significant pesticides, namely paraoxon and chlorpyrifos. TGO@UiO-66 by providing a high surface area and excellent conductivity facilitated the electron transfer between the analyte and the electrode surface. The designed sensor exhibited a wide linear range with low limits of detection, fast response and also satisfying stability and reproducibility for the determination of POX and CPF. The application of the proposed sensor for the determination of organophosphorus pesticides in different real samples was also examined and highly satisfactory results were achieved.

Conflicts of interest

There are no conflicts to declare.

Acknowledgements

References

1 Y.-M. Ho, Y.-K. Tsoi and K. S.-Y. Leung, *Anal. Chim. Acta*, 2013, **775**, 58–66.

2 J. Mehta, P. Vinayak, S. K. Tuteja, V. A. Chhabra, N. Bhardwaj, A. Paul, K.-H. Kim and A. Deep, *Biosens. Bioelectron.*, 2016, **83**, 339–346.

3 R. B. Dominguez, G. A. Alonso, R. Muñoz, A. Hayat and J.-L. Marty, *Sens. Actuators, B*, 2015, **208**, 491–496.

4 G. Briceño, H. Schalchli, O. Rubilar, G. Tortella, A. Mutis, C. S. Benimeli, G. Palma and M. Diez, *Chemosphere*, 2016, **156**, 195–203.

5 R. K. Mishra, G. A. Alonso, G. Istamboulie, S. Bhand and J.-L. Marty, *Sens. Actuators, B*, 2015, **208**, 228–237.

6 P. Kumar, K.-H. Kim and A. Deep, *Biosens. Bioelectron.*, 2015, **70**, 469–481.

7 Z. O. Uygun and Y. Dilgin, *Sens. Actuators, B*, 2013, **188**, 78–84.

8 T. C. Kwong, *Ther. Drug Monit.*, 2002, **24**, 144–149.

9 S. Feng, Y. Hu, L. Ma and X. Lu, *Sens. Actuators, B*, 2017, **241**, 750–757.

10 M. Guler, V. Turkoglu and Z. Basi, *Electrochim. Acta*, 2017, **240**, 129–135.

11 H. Mao, Z. Zuo, N. Yang, J. S. Huang and Y. Ya, *J. Residuals Sci. Technol.*, 2017, **14**, 255–269.

Table 1 Simultaneous determination of POX and CPF in tap water and vegetable samples

Sample	Added (nM)	Found[a] (nM)	Recovery%	RSD%
Tap water	50.0	48.7	97.4	3.2
	60.0	108.9	99.0	2.8
	70.0	182.4	101.3	4.1
Celery	50.0	50.9	101.8	3.7
	60.0	112.5	102.2	3.9
Lettuce	70.0	177.4	98.5	2.8
	50.0	52.8	105.6	1.9
	60.0	106.8	97.0	2.5
	70.0	186.3	103.5	3.8
Cabbage	50.0	53.2	106.4	2.6
	60.0	116.4	105.8	3.2
	70.0	174.9	97.1	4.1

[a] Each value is the average of three determinations.

12 F. Arduini, M. Forchielli, A. Amine, D. Neagu, I. Cacciotti, F. Nanni, D. Moscone and G. Palleschi, *Microchim. Acta*, 2015, **182**, 643–651.

13 J. Turan, M. Kesik, S. Soylemez, S. Goker, S. Coskun, H. E. Unalan and L. Toppare, *Sens. Actuators, B*, 2016, **228**, 278–286.

14 T. Wang, J. Wang, Y. Yang, P. Su and Y. Yang, *Ind. Eng. Chem. Res.*, 2017, **56**, 9762–9769.

15 Y. Cao, X. Sun, Y. Guo, W. Zhao and X. Wang, *Bioprocess Biosyst. Eng.*, 2015, **38**, 307–313.

16 M. Pohanka, M. Hrabinova, J. Fusek, D. Hynek, V. Adam, J. Hubalek and R. Kizek, *Int. J. Electrochem. Sci.*, 2012, **7**, 50–57.

17 J. M. Zen, A. Senthil Kumar and D. M. Tsai, *Electroanalysis*, 2003, **15**, 1073–1087.

18 P. Chandra, H.-B. Noh, M.-S. Won and Y.-B. Shim, *Biosens. Bioelectron.*, 2011, **26**, 4442–4449.

19 P. D. Johnson, P. Girinathannair, K. N. Ohlinger, S. Ritchie, L. Teuber and J. Kirby, *Water Environ. Res.*, 2008, **80**, 472–479.

20 J. Zheng, Y. He, Q. Sheng and H. Zhang, *J. Mater. Chem.*, 2011, **21**, 12873–12879.

21 L. Wang, J. Bai, X. Bo, X. Zhang and L. Guo, *Talanta*, 2011, **83**, 1386–1391.

22 D. Yang, S. O. Odoh, T. C. Wang, O. K. Farha, J. T. Hupp, C. J. Cramer, L. Gagliardi and B. C. Gates, *J. Am. Chem. Soc.*, 2015, **137**, 7391–7396.

23 C. G. Piscopo, F. Trapani, A. Polyzoidis, M. Schwarzer, A. Pace and S. Loebbecke, *New J. Chem.*, 2016, **40**, 8220–8224.

24 T. Gan, J. Sun, W. Meng, L. Song and Y. Zhang, *Food Chem.*, 2013, **141**, 3731–3737.

25 J. Hao, K. Wu, C. Wan and Y. Tang, *Talanta*, 2018, **185**, 550–556.

26 Y. Fan, K.-J. Huang, D.-J. Niu, C.-P. Yang and Q.-S. Jing, *Electrochim. Acta*, 2011, **56**, 4685–4690.

27 A. Kumaravel and M. Chandrasekaran, *J. Agric. Food Chem.*, 2015, **63**, 6150–6156.

28 J. Ding, Z. Yang, C. He, X. Tong, Y. Li, X. Niu and H. Zhang, *J. Colloid Interface Sci.*, 2017, **497**, 126–133.

29 N. I. Kovtyukhova, P. J. Ollivier, B. R. Martin, T. E. Mallouk, S. A. Chizhik, E. V. Buzaneva and A. D. Gorchinskiy, *Chem. Mater.*, 1999, **11**, 771–778.

30 F. Yang, W. Li and B. Tang, *J. Alloys Compd.*, 2018, **733**, 8–14.

31 C. Petit and T. J. Bandosz, *Adv. Mater.*, 2009, **21**, 4753–4757.

32 C. Petit and T. J. Bandosz, *J. Mater. Chem.*, 2009, **19**, 6521–6528.

33 A. Crake, K. C. Christoforidis, A. Kafizas, S. Zafeiratos and C. Petit, *Appl. Catal., B*, 2017, **210**, 131–140.

34 A. Mardiroosi, A. R. Mahjoub and H. Fakhri, *J. Mater. Sci.: Mater. Electron.*, 2017, **28**, 11722–11732.

35 R. Mehek, N. Iqbal, T. Noor, H. Nasir, Y. Mehmood and S. Ahmed, *Electrochim. Acta*, 2017, **255**, 195–204.

36 Y. Chen, D. Lv, J. Wu, J. Xiao, H. Xi, Q. Xia and Z. Li, *Chem. Eng. J.*, 2017, **308**, 1065–1072.

37 J. Ma, X. Guo, Y. Ying, D. Liu and C. i. Zhong, *Chem. Eng. J.*, 2017, **313**, 890–898.

38 C. Zhu, K. Wang, T. Lei, T. Xiao and L. Liu, *Mater. Lett.*, 2018, **216**, 243–247.

39 Y. Cao, Y. Zhao, Z. Lv, F. Song and Q. Zhong, *J. Ind. Eng. Chem.*, 2015, **27**, 102–107.

40 D. Cai and M. Song, *J. Mater. Chem.*, 2007, **17**, 3678–3680.

41 V. Jabbari, J. M. Veleta and M. Zarei-Chaleshtori, *Chem. Eng. J.*, 2016, **304**, 774–783.

42 X. Zhou, W. Huang, J. Shi, Z. Zhao, Q. Xia, Y. Li, H. Wang and Z. Li, *J. Mater. Chem. A*, 2014, **2**, 4722–4730.

43 N. Sreedhar, M. S. Kumar and K. Krishnaveni, *Sens. Actuators, B*, 2015, **210**, 475–482.

44 T. Alizadeh, *Thin Solid Films*, 2010, **518**, 6099–6106.